

Reconstruction of Multi-Energy X-Ray Computed Tomography Images of Laboratory Mice¹

S.S. Gleason², *Member IEEE*, H. Sari-Sarraf², *Member IEEE*, M. J. Paulus², *Member IEEE*, D. K. Johnson², S. J. Norton², and M. A. Abidi³, *Member IEEE*

²Oak Ridge National Laboratory, P.O. Box 2008, Oak Ridge, Tennessee 37831-6011

³The University of Tennessee, Electrical Engineering Department, Knoxville, Tennessee, 37996-2100

Abstract

A new x-ray computed tomography (CT) system is being developed at Oak Ridge National Laboratory to image laboratory mice for the purpose of rapid phenotype screening and identification. One implementation of this CT system allows simultaneous capture of several sets of sinogram data, each having a unique x-ray energy distribution. The goals of this paper are to (1) identify issues associated with the reconstruction of this energy-dependent data and (2) suggest preliminary approaches to address these issues. Due to varying numbers of photon counts within each set, both traditional (filtered backprojection, or FBP) and statistical (maximum likelihood, or ML) tomographic image reconstruction techniques have been applied to the energy-dependent sinogram data. Results of reconstructed images using both algorithms on sinogram data (high- and low-count) are presented. Also, tissue contrast within the energy-dependent images is compared to known x-ray attenuation coefficients of soft tissue (e.g. muscle, bone, and fat).

I. INTRODUCTION

The Oak Ridge National Laboratory (ORNL) has a world class Mammalian Genetics Research Facility that houses more than 70,000 mice representing about 400 mutant lines. Mutagenesis experiments are performed on the mice, and it is important to then determine the physical manifestations (phenotypes) of these induced mutations. These phenotypes are often difficult to find, especially when only a few researchers are available to screen a large number of mice. A large percentage of these phenotypes are expressed as internal abnormalities that cannot be seen without sacrificing the mouse. Examples of these phenotypes include skeletal deformities (e.g. scoliosis) and deformed or diseased organs (e.g. polycystic kidney disease).

A Laboratory-Directed Research and Development (LDRD) program was recently started at ORNL with the objective of accelerating the process of screening these mice for internal abnormalities. A new high-resolution, x-ray CT instrument called MicroCAT is under development as a part of this new program. A complete description of the MicroCAT hardware is given in [1] along with a few sets of example images, the majority of which were captured using a CCD-based mammography-type sensor. This paper focuses strictly on the implementation of this instrument that employs a cadmium zinc telluride (CZT) sensor and is capable of simultaneously capturing several sets of sinogram data, each containing a specific band, or bin, of x-ray energies. These individual energy-dependent sinograms contain varying number of photon counts depending on the x-ray source energy spectrum.

The cumulative x-ray sinogram (sum of all energy bins) typically has a reasonable number of counts (thousands) and images can be reconstructed with relatively good quality via FBP [2] (see Fig. 1). The energy bins at the ends of the source spectrum, however, typically have very low photon counts (60-100), and are therefore good candidates for statistical or probabilistic reconstruction techniques. Statistical techniques for x-ray transmission tomography have not received as much attention as statistical techniques for emission tomography applications such as PET and SPECT. There are, however, several promising approaches that have been developed for transmission imaging in cases where low statistics are common [3-6].

This paper first discusses the characteristics of the energy-dependent sinogram data. It then presents examples of images reconstructed at each energy level using FBP and a variation of the maximum likelihood algorithm [5]. In addition, it compares the relative tissue intensities within reconstructed images to published x-ray attenuation coefficients of bone, soft tissue, and fat [7] (see Fig. 2). Finally, it introduces some future research topics in tomographic image reconstruction that utilize the multi-energy capability of this new CT scanner to further enhance the information content of the reconstructed images.

¹Research sponsored by the Laboratory Directed Research and Development Program of Oak Ridge National Laboratory, managed by Lockheed Martin Energy Research Corp. for the U.S. Department of Energy under Contract No. DE-AC05-96OR22464.

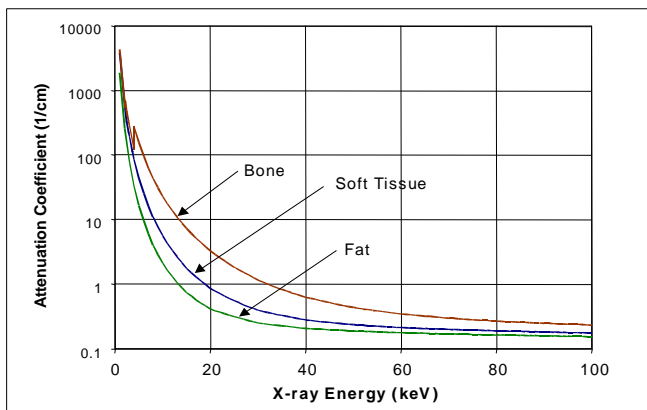


Figure 2. Plot showing how attenuation coefficients vary according to x-ray energy for three different tissue types.

II. MULTI-ENERGY CT

When configured for energy-dependent data acquisition, the MicroCAT employs a single-element CZT detector with a 100 μm diameter collimator. The read-out electronics for this detector are described in [1]. We have recently purchased a new custom 2-sided CZT strip detector and are completing the design of the custom read-out electronics. This CZT array will then be used in a cone beam configuration to perform energy-dependent scans at a much faster rate than currently possible.

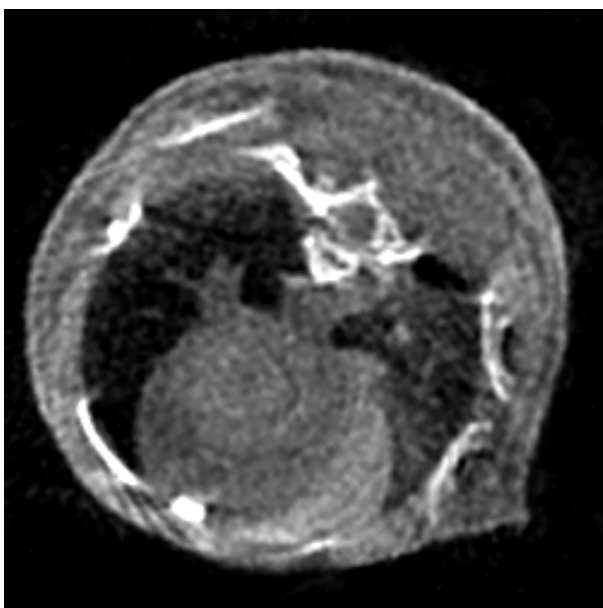


Figure 1. Cumulative energy image of mouse thorax reconstructed using FBP. The heart, thymus, lungs, spinal column, spinal cord, sternum, and several ribs are visible.

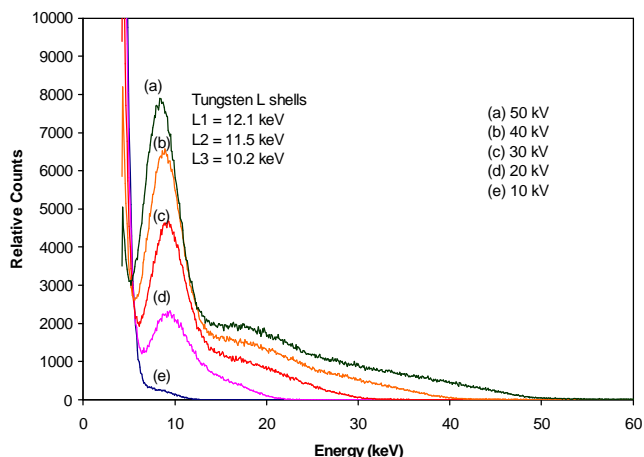


Figure 3. The measured source spectra for the MicroCAT tungsten x-ray source. Bias voltages of 10-50 kVp are shown. Note that the noise floor is around 7-8 keV.

X-ray Source

The x-ray source is a 50W mini-focus (<200 μm spot) tungsten-anode tube with variable anode voltage (10-50 kVp) and current (0.1 - 1 mA). The measured energy spectrum for the incident polychromatic x-ray source is shown in Fig. 3. As discussed in more detail in [1], the spectra were measured using the single-element CZT detector and a 1024 channel multi-channel analyzer (MCA). The MCA was calibrated using Cd-109 and Am-241 test sources.

Energy-Dependent Data Collection

Before the subject is scanned, the user can select up to ten x-ray energy bins in which to collect the x-ray photons. As the subject is scanned, the individual x-rays are counted and put into the proper bin depending on their energy level. As shown in Fig. 2, different tissue types in the body have significantly varied x-ray attenuation coefficients for low-energy x-rays [7]. Note that the largest difference between attenuation coefficients of the tissues occurs in the lower energy range (10 - 30 keV). When scanning the human chest, these low-energy x rays are not used exclusively because they would be entirely absorbed within the body. Mice, on the other hand, are small enough that an adequate number of these low-energy x rays can pass through the body of the mouse and subsequently be detected on the other side.

By reconstructing images from sinogram data within a specific energy band, one can accomplish certain computer-aided diagnostic tasks that may otherwise be difficult and/or time consuming. For example, if one is trying to differentiate two tissue types with similar mass density, standard energy-integrating x-ray scans will not provide adequate contrast. If,

however, the two tissues have different chemical compositions (i.e. breast tissue and microcalcifications), then multi-energy data can be used to determine Compton scattering and photoelectric effects separately. These effects can be used to provide contrast between the tissue types of interest for diagnostic purposes. This is addressed in more detail in Section IV. The next section describes two reconstruction approaches and presents example images reconstructed with energy-dependent sinogram data.

Limited Statistics

The implementation of the MicroCAT scanner used in this study has certain characteristics that cause it to suffer from limited statistics. First, the single-element CZT detector had to be mechanically translated to every position within the sinogram space. Because of scanning time constraints, the detector was stationary for only 0.1 seconds at each position, and this limited the number of x rays that could be counted. Second, a 100 μm collimator reduced the solid angle of collection significantly, reducing the number of x rays incident on the detector during that 0.1 sec. exposure. Finally, the x-ray photon counts were divided into energy-dependent bins. Each bin, of course, has only a fraction of the total collected x-ray counts, further limiting the signal statistics. These limitations can be overcome in future versions of the scanner through, for example, the use of a higher-powered x-ray source. As is the case for nuclear modalities such as PET or SPECT, the limited-count, energy-dependent sinograms are good candidates for statistical or probabilistic image reconstruction approaches, as described in the following section.

It has been shown by Kak *et al.* [8] that the variance of the noise in an FBP-reconstructed image is inversely proportional to both the number of projections taken during a scan and the number of detected x-ray photons exiting the object being scanned. This is one reason that textured noise becomes prominent when reconstructing low-count projection data via FBP (see Fig. 5, 30 - 45 keV). Also, poor statistics are a significant problem for transmission imaging because the data undergo a nonlinear transformation before reconstruction. As noted by Ollinger [4], this can introduce both singularities and systematic bias in the estimated line integrals through the subject being scanned. Although the mathematically exact FBP is the method of choice for reconstructing projection data with good statistics, iterative reconstruction approaches such as ML-EM will eliminate these undefined (singular) and biased line integrals. Finally, in ML-based reconstruction techniques, the use of a Poisson model for the source and detector is an accurate one and helps to constrain the final reconstruction solution to achieve reasonable results when confronted with limited statistics.

III. RECONSTRUCTION ALGORITHMS

This section briefly describes the two image reconstruction approaches used to generate the CT slice images presented herein. Both FBP and an iterative ML algorithm called the convex algorithm [5] were implemented and tested on the energy-dependent sinograms.

The 200 x 200 image shown in Fig. 1 was reconstructed using FBP with a standard ramp filter. No additional filtering was applied. The sinogram data passed to the reconstruction algorithm were the cumulative sums of all energies detected. The sinogram was composed of 225 projections, 0.8 degrees apart, with 200 samples per projection. Typical photon counts per detector were in the thousands. The x-ray source is a fan-beam, and the sinogram data were resorted into a parallel beam configuration before submitting them to the parallel FBP reconstruction algorithm. The resolution of the resultant image is approximately 250 μm per pixel. This image took approximately 12 seconds to reconstruct on a 266 MHz PC using standard, but unoptimized, FBP routines.

The ML reconstruction method published in [5] was also implemented in anticipation of x-ray sinograms with poor statistics. For ML reconstruction in transmission tomography a Poisson model is used for the source and the detector to formulate a log-likelihood function as follows:

$$L(\mu) = \sum_i (-d_i e^{-\langle l_i, \mu \rangle} - Y_i \langle l_i, \mu \rangle) + c, \quad (1)$$

where μ is the vector of attenuation coefficients for the reconstructed image, d_i is the expected number of photon counts leaving the source along projection path i , Y_i represents the observed photon counts, and c represents terms that are independent of μ . Also, $\langle l_i, \mu \rangle$ denotes the inner product of l_i and μ , and l is a matrix of intersection lengths, where l_{ij} is the intersection length of projection i with pixel j . Direct maximization of $L(\mu)$ is difficult, so, using the convex properties of L , one can re-pose the likelihood function as a new function $Q(\mu)$ that maximizes at the same value of μ as does $L(\mu)$. The iterative solution is:

$$\mu_j^{n+1} = \mu_j^n + \frac{\mu_j^n \sum_i l_{ij} [d_i e^{-\langle l_i, \mu_n \rangle} - Y_i]}{\sum_i l_{ij} \langle l_i, \mu_n \rangle d_i e^{-\langle l_i, \mu_n \rangle}}. \quad (2)$$

Fig. 4 shows the result of 30 iterations of the convex algorithm on the same sinogram data used to generate the FBP image in Fig. 1. The convex algorithm took about 15 minutes to run on a 266 MHz PC. Because image appearance, not execution time, was the primary objective in this work, the convex algorithm was implemented accurately, but not efficiently. There are several implementation changes that could be made to speed up the algorithm by an order of

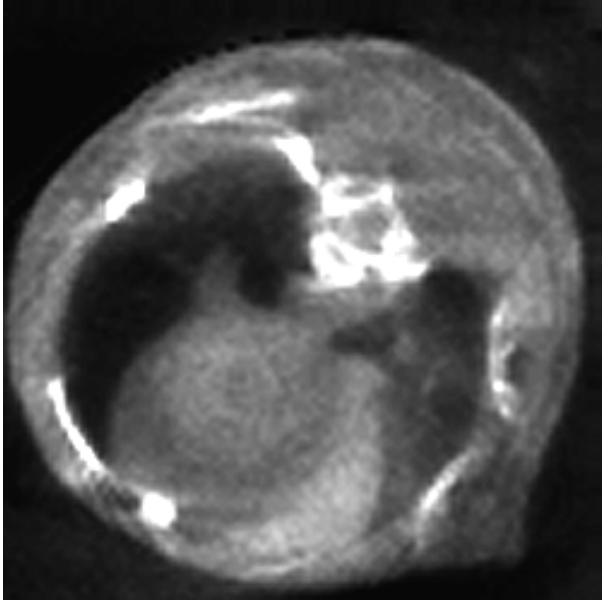


Figure 4. Result after 30 iterations of the ML-based convex reconstruction algorithm.

magnitude (see results presented in [5]). The overall quality of the images in Fig. 1 and Fig. 4 is reasonable in terms of visible detail and contrast between structures. The FBP image has slightly more textured noise than the convex image, but also has more crisply defined edges between organs. Because the statistics of the cumulative-count sinogram are good, both reconstruction algorithms generate reasonable results. We now turn our attention to energy-dependent sinograms.

Fig. 5 shows six images reconstructed using FBP on energy-dependent sinograms. The two most interesting aspects of the images in Fig. 5 are: (1) the increased noise level and (2) the varying tissue contrasts across the energy-dependent images. Because of the limited x-ray photon counts within each energy band, the FBP algorithm generates significant textured noise in the reconstructed image.

The ring artifacts within the image are most likely the result of a non-optimal calibration procedure that introduced small offset errors into the photon counts recorded at particular detector positions. The calibration data set (I_0) was recorded for a single projection, and then used to normalize every projection (225 in this case) captured during the scan of a subject. Although this is standard practice, it is believed that projection-dependent electronic noise may have introduced these small offset errors that lead to ring artifacts in the reconstructed image. With large photon counts, the rings are almost imperceptible, but when the statistics are extremely poor, the ring artifacts are quite prominent (e.g.

see Fig. 5, 30 - 45 keV). If one can “look through” the textured noise, there are visible anatomical details within each of the six energy bands.

It is interesting to compare the x-ray energy range of each image to the attenuation coefficient plot shown in Fig. 2. For example, the first image in Fig. 5 (0 - 7.5 keV) shows little difference in attenuation coefficient between bone and soft tissue (e.g. heart muscle). This corresponds well to the attenuation coefficients within the corresponding energy range in Fig. 2. Note that below 5 keV, the attenuation coefficients of bone, soft tissue and fat begin to converge. The next four energy bands (7.5 - 15, 15 - 22.5, 22.5 - 30, and 30 - 37.5 keV) all correspond to areas in Fig. 2 where the respective attenuation coefficients are significantly different. In the last image of Fig. 5 (energy band 37.5 - 45 keV), one can see that the attenuation values are again beginning to converge. This also agrees with the attenuation curves in Fig. 2.

To illustrate the utility of an iterative reconstruction algorithm on low-count, x-ray sinogram data, the convex algorithm was applied to the same sinogram data sets. The result of 30 iterations of the convex algorithm on these six data sets is shown in Fig. 6. There is an advantage in using the convex algorithm in terms of textured noise reduction that leads to a more homogeneous intensity within the individual organs. On the other hand, edges between structures are clearer in the FBP images. In the highest energy bins (30 - 45 keV) the convex algorithm reconstructs images in which the heart, lungs, thymus, and spinal column are discernible, yet blurry. In the corresponding FBP images, the textured noise pattern overwhelms the organ contrast, and, in particular, the heart, thymus, and right lung become very difficult to differentiate. This is not surprising, given that iterative reconstruction techniques are often used successfully to reconstruct low-resolution images using data with poor statistics [9-11]. Finally, similar to the FBP images, the images reconstructed via the convex algorithm show a good correspondence between tissue intensity differences and the attenuation coefficients plotted in Fig. 2.

IV. FUTURE RESEARCH

Reconstruction of energy-dependent sinogram data could be further exploited in several conceivable ways. The simplest approach is the one presented in this paper, that is, to generate separate images at different x-ray energies with the expectation that subtle differences in tissue types or abnormalities could be enhanced at different energies. This idea could be extended by selecting, for example, a linear combination of the images reconstructed at different energies to enhance the contrast between two specific tissue types of interest (e.g., fat and soft tissue). More sophisticated

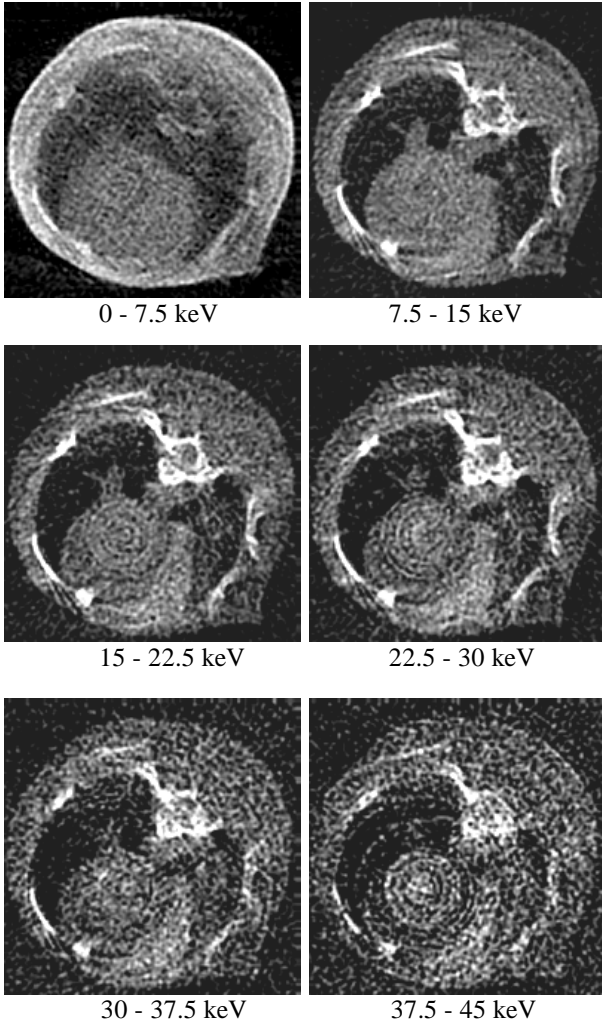


Figure 5. FBP-reconstructed images from energy-dependent sinogram data. X-ray energies within each band are listed under the corresponding image.

image fusion techniques should be investigated to make better use of the energy-dependent image data.

Another possibility was proposed by Alvarez and Macovski [12], but was implemented only on simulated data due to the unavailability of energy-dependent CT machines. Their idea was to exploit the different energy dependencies of the two primary x-ray interaction mechanisms, Compton scattering and photoelectric absorption, to display separate images of these interactions. That is, the energy-dependence of the attenuation coefficient may be written:

$$\mu(x, y, E) = \mu_{PE}(x, y)f_{PE}(E) + \mu_{CS}(x, y)f_{CS}(E), \quad (3)$$

where $f_{PE}(E)$ and $f_{CS}(E)$ are known functions of energy associated with the photoelectric and Compton scattering interactions, respectively. With a CT system capable of

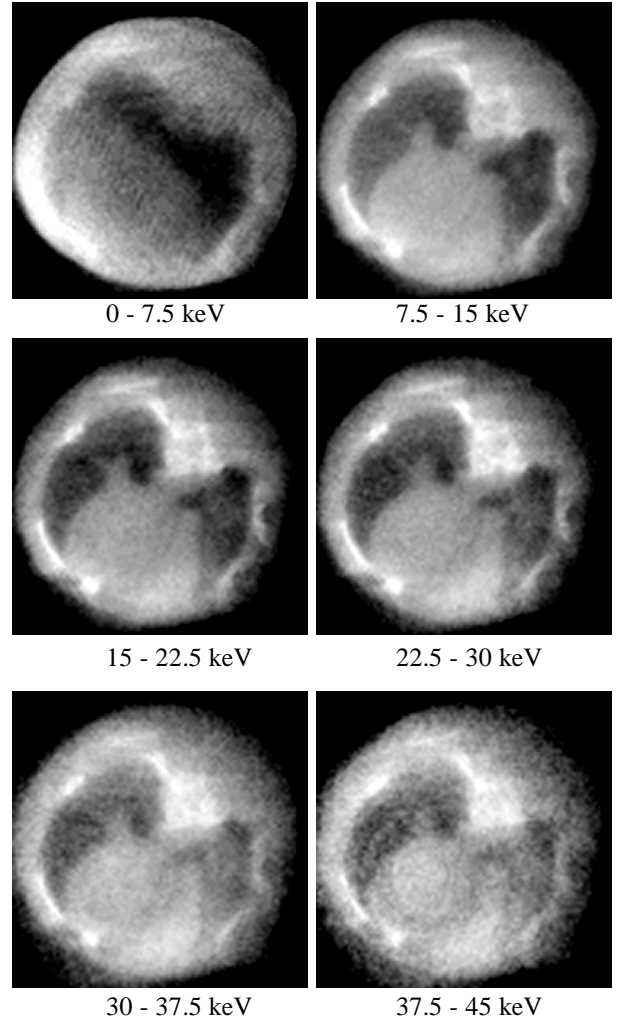


Figure 6. Images reconstructed using the convex algorithm from energy-dependent sinogram data. X-ray energies within each band are listed under the corresponding image.

energy resolution, separate images of $\mu_{PE}(x, y)$ and $\mu_{CS}(x, y)$ can be reconstructed. The importance of displaying such images stems from the fact that the photoelectric interaction, conveyed by $\mu_{PE}(x, y)$, is a strongly increasing function of atomic number and thus reflects the molecular composition of the tissue type. Compton scattering, conveyed by $\mu_{CS}(x, y)$, depends on the electron density, which is related to the mass density of the tissue. Separate images of these interaction mechanisms would almost certainly provide information of new diagnostic value. A potentially important example is breast cancer detection, wherein a purely photoelectric image should enhance the contrast between the soft tissue in the breast and the microcalcifications that are the precursors to cancer. We intend to implement and evaluate the method described above using the CZT-based, CT system. Because of the potentially poor sta-

tistics (i.e., low x-ray photon counts) experienced to-date using the CZT-based system, it will also be necessary to derive a novel solution for this new reconstruction method that employs probabilistic techniques based on the ML technique.

V. CONCLUSION

This paper has presented the results of performing multi-energy, x-ray computed tomography with a unique instrument employing a CZT x-ray detector. The energy-dependent sinograms generated by this system were reconstructed using both the FBP and ML-based, convex reconstruction algorithms. As anticipated, the convex reconstruction algorithm proved useful when the x-ray photon statistics within an energy band were limited. Also, in energy bands where a reasonable number of photon counts were available, FBP generated quality images with crisp delineation between internal structures (bone and soft tissues). The intensity variation between tissue types within all of the energy-dependent images corresponds well with the expected energy-dependent attenuation coefficients for bone and soft tissues.

There are many opportunities for further research in terms of both energy-dependent image analysis as well as energy-dependent image reconstruction techniques. Current efforts are underway to more effectively use energy-dependent data sets to reconstruct separate images of photoelectric absorption and Compton scatter interactions. These images will allow the end user to better discriminate between tissue types for the purposes of, for example, phenotype identification.

VI. ACKNOWLEDGEMENTS

The authors would like to thank the reviewers for their comments and suggestions that lead to several substantial improvements in this paper.

VII. REFERENCES

- [1]. M. J. Paulus, H. Sari-Sarraf, S. S. Gleason, M. Bobrek, J. S. Hicks, D. K. Johnson, J. K. Behel, and L. H. Thompson, "A New X-ray Computed Tomography System for Laboratory Mouse Imaging," Submitted to *IEEE Trans. on Nucl. Science*, 1999.
- [2]. G. T. Herman, *Image Reconstruction from Projections: The Fundamentals of Computerized Tomography*, New York: Academic Press, 1980.
- [3]. K. Lange and R. E. Carson, "EM Reconstruction Algorithms for Emission and Transmission Tomography," *J. of Computer Asst. Tomogr.*, pp. 306-16, April 1984.
- [4]. J. M. Ollinger, "Maximum-Likelihood Reconstruction of Transmission Images in Emission Computed Tomography via the EM Algorithm," *IEEE Trans. on Medical Imaging*, vol. 13, no. 1, March 1994.
- [5]. K. Lange and J. A. Fessler, "Globally Convergent Algorithms for Maximum a Posteriori Transmission Tomography," *IEEE Trans. on Image Proc.*, vol. 4, no. 10, October 1995.
- [6]. H. A. Erdogan and J. A. Fessler, "Fast Monotonic Algorithms for Transmission Tomography," *IEEE Trans. on Med. Imag.*, submitted, May 1998.
- [7]. ICRU, "Tissue Substitutes in Radiation Dosimetry and Measurement," Report 44 of the International Commission on Radiation Units and Measurements, Bethesda, MD, [www:http://physics.nist.gov/PhysRefData/XrayMassCoef/tab2.html](http://physics.nist.gov/PhysRefData/XrayMassCoef/tab2.html), 1989.
- [8]. A. C. Kak, M. Slaney, *Principles of Computerized Tomographic Imaging*, IEEE Press, New York, 1988.
- [9]. L. A. Shepp and Y. Vardi, "Maximum Likelihood Reconstruction for Emission Tomography," *IEEE Trans. on Med. Imag.*, vol. MI-1, no. 2, pp. 113-122, October 1992.
- [10]. J. M. Ollinger and J. A. Fessler, "Positron Emission Tomography," *IEEE Signal Processing Magazine*, pp. 43-54, January 1997.
- [11]. C. A. Johnson, J. Seidel, R. E. Carson, W. R. Gandler, A. Sofer, M. V. Green, M. E. Daube-Witherspoon, "Evaluation of 3D Reconstruction Algorithms for a Small Animal PET Camera," *Proc. IEEE 1996 Medical Imaging Conf.*, November 1996.
- [12]. R. E. Alvarez and A. Macovski, Energy-selective reconstruction in X-ray computerized tomography, *Phys. Med. Biol.*, 21, 733-744, 1976.